The Journal of Chemical Physics

Gold nanoparticle distribution in polyelectrolyte brushes loaded at different pH conditions

Cite as: J. Chem. Phys. **149**, 163322 (2018); https://doi.org/10.1063/1.5035554
Submitted: 16 April 2018 • Accepted: 15 June 2018 • Published Online: 18 July 2018

Dikran Boyaciyan, Larissa Braun, Oliver Löhmann, et al.

THE JOURNAL OF CHEMICAL PHYSICS **149**, 163322 (2018)

Gold nanoparticle distribution in polyelectrolyte brushes loaded at different pH conditions

Dikran Boyaciyan,[1] Larissa Braun,[1] Oliver Löhmann,[1] Luca Silvi,[2] Emanuel Schneck,[3] and Regine von Klitzing[1]
[1]*Soft Matter at Interfaces, Technische Universität Darmstadt, Alarich-Weiss-Straße 10, 64287 Darmstadt, Germany*
[2]*Helmholtz-Zentrum Berlin für Materialien und Energie, Hahn-Meitner-Platz 1, 14109 Berlin, Germany*
[3]*Max Planck Institute of Colloids and Interfaces, Department of Biomaterials, Am Mühlenberg 1, 14476 Potsdam, Germany*

(Received 16 April 2018; accepted 15 June 2018; published online 18 July 2018)

Composites made of polymer brushes with inclusions of gold nanoparticles (AuNPs) combine the responsive nature of polymer brushes with the optical properties of the AuNPs, which offers the possibility to be used as colorimetric sensors. To this end, it is crucial to know how AuNPs are distributed inside the brush. Here, this distribution was elucidated by neutron reflectometry with contrast variation and a self-consistent reflectivity analysis based on the analytical parameterization of the volume fraction profiles of all chemical components. In contrast to former studies, this analysis allows the determination of the spatial distribution of components separately from each other: polyelectrolyte, AuNP, and water. Cationic poly-[2-(Methacryloyloxy) ethyl] trimethylammonium chloride (PMETAC) brushes were loaded with 5 nm AuNPs, which were coated with a pH-sensitive capping. The pH was varied during the incubation of the brush in the AuNP suspension. At a lower pH, AuNPs form aggregates in suspension and are attached to the brush periphery. They adsorb into the brush but do not fully penetrate it due to their bulkiness. At a higher pH, AuNP suspensions are electrostatically stabilized and the AuNPs penetrate the brush entirely. However, the AuNP distribution over the brush is not homogeneous but decreases gradually toward the substrate. Penetration of the AuNPs leads to a more extended conformation of the brush. According to the results of the detailed analysis of all components, an increase in water content could be excluded as a reason for brush swelling but replacement of water by the AuNP was observed. *Published by AIP Publishing.*
https://doi.org/10.1063/1.5035554

I. INTRODUCTION

Surface modification with polymers has received great attention in soft matter science in context with the development of nanomaterials with customized properties.[1,2] Prominent examples are polymer brushes[3,4] consisting of polymer chains, which are chemically end-grafted to a substrate. They can be applied to flat,[5–7] spherical,[8–10] or porous[11–13] substrates. The surface properties can be easily tailored by changing the chain functionality.[14–16] Their potential, in particular, lies in the sensitivity to external stimuli[17,18] so that they are suitable for numerous technological applications. Due to the optical transparency of the polymer brushes, one promising application is colorimetric sensors realized by embedding optically functional nanoparticles into stimuli-responsive polymer brushes. Gold nanoparticles (AuNPs), for instance, exhibit a surface plasmon resonance (SPR) so that environmental changes can be detected spectroscopically.[19,20] Namely, when the conformation of the brush responds to a chemical stimulus (the analyte), it triggers a change in the proximity of the AuNPs, in turn resulting in a spectral shift.

With respect to sensor applications, Fortin and Klok[21] grafted polymer brushes inside polypropylene hollow fibers in order to monitor the glucose level of the environment. Poly(methacrylic acid) (PMAA) brushes were functionalized with phenylboronic acid (PBA) that can bind glucose. The experiments revealed that glucose concentration down to 10 mM can be detected. Therefore, polypropylene hollow fibers modified with polymer brushes can be considered for sensing blood glucose levels of diabetic patients. Ferhan *et al.*[22] used polymer brushes for the incorporation of AuNPs for the spectroscopic detection of lead ions. Poly(oligo(ethylene glycol) methacrylate) (POEGMA) brushes were grown on glass and loaded with AuNPs. As a post-functionalization, AuNPs were coated with thiosulfate. By exposing POEGMA/AuNP composites to lead ions, formation of nanoparticles with the Au-PB alloy surface occurs, which leads to a reduced interaction with the polymer brush and particle release from the brush matrix, which in turn was detected by a decrease in UV/Vis absorbance.

As a basis for the rational design of composite materials with desired properties and to be used as colorimetric sensors, it is important to control the AuNP distribution over the brush and characterize the composites' internal structure. An effort has been made previously[23] using neutron reflectometry (NR) and X-ray reflectometry (XRR) to elucidate the

distribution of AuNPs. The AuNPs had a pH-sensitive capping with 3-mercaptopropionic acid (MPA) and were embedded into a strong positively charged poly-[2-(Methacryloyloxy) ethyl] trimethylammonium chloride (PMETAC) brush at different pH. First of all, it could be shown that a pH-insensitive brush becomes pH-sensitive after loading with the capped AuNPs.[24] Second, there is a strong hint that the distribution of AuNPs can vary with pH from a rather 2D assembly at the brush surface to a more 3D distribution within the brush. However, in order to control the AuNP distribution, more detailed information about the composites' internal structure is required. The incorporation of AuNPs changes not only the water content but also the brush conformation. So far, it was impossible to separate those two effects.

In the present paper, the same composite of PMETAC brushes loaded with MPA capped AuNPs is investigated with a focus on the AuNP distribution within the brush. For this purpose, NR was carried out against several water contrasts and analyzed with the help of a self-consistent model based on the analytical parameterization of the volume fraction profiles of all chemical components. This approach yields much more detailed information on the internal structure of the composites than previous studies. AuNPs at pH 4 are attached to the brush periphery as aggregates without deeply penetrating the PMETAC brush. By contrast, at pH 8, AuNPs penetrate the brush completely. Under both pH conditions, the PMETAC brushes become more elongated upon AuNP distribution.

II. EXPERIMENTAL SECTION

A. Materials

2-(methacryloyloxy)ethyl-trimethylammonium chloride (METAC), 2,2′-Bipyridine, copper(I) chloride (CuCl), copper(II) chloride ($CuCl_2$), sulfuric acid (H_2SO_4), hydrogen peroxide (H_2O_2), gold(III) chloro trihydrate ($HAuCl_4 \times 3\ H_2O$), sodium borohydride ($NaBH_4$), sodium citrate trihydrate, 3-mercaptopropionic acid (MPA), thioctic acid, sodium hydroxide (NaOH), formic acid, potassium hydroxide (KOH), trishydroxymethylaminomethane (TRIS), hydrogen chloride (HCl), ethanol (EtOH), methanol (MeOH), and toluene were purchased from Sigma-Aldrich (St. Louis, MO, USA) and used without further purification. Silicon blocks with dimensions of 5 cm × 8 cm × 1.5 cm with a roughness less than 0.2 nm were used for neutron reflectometry measurements and purchased from Siltronic AG (München, Germany).

B. Synthesis and preparation

1. PMETAC brushes

Before synthesis, the substrates were etched for 30 min using piranha solution (H_2SO_4/H_2O_2 1:1 v/v%) to clean the surface and generate free hydroxyl groups at the surface. The freshly cleaned substrates were incubated into a 2-bromo-2-methyl-N-(3-(triethoxysilyl)propyl)propanamide (BTPAm) and dry toluene solution (4 μl/10 ml BTPAm/dry Toluene) for 24 h at room temperature to generate a monolayer of BTPAm on the substrate. BTPAm was synthesized according to the literature procedure.[25] After deposition, the substrates were sonicated in toluene for 20 min, rinsed with EtOH, and dried under a stream of nitrogen.

The synthesis of PMETAC brushes was modified from the literature[26] as follows: METAC (154 ml, 660 mmol) was mixed with 2,2′-bipyridyl (3.714 g, 23.8 mmol) in 88 mL of Milli-Q water/MeOH (1:4 v/v%). The mixture was flushed with N_2 for 30 min. Then, CuCl (1.437 g, 14.5 mmol) and $CuCl_2$ (132 mg, 0.97 mmol) were added quickly to the mixture. The mixture was further stirred and degassed for another 30 min. The BTPAm-coated substrates were placed in the reactor in nitrogen atmosphere. The polymerization was stopped after 1.5 h at room temperature by exposing the samples to air. The samples were sonicated in water for 10 min, then in MeOH for another 10 min, and dried with nitrogen. The thickness of the PMETAC brush under ambient conditions (≈30% RH) was 212 ± 13 Å with a refractive index of 1.52 determined by ellipsometry.

2. 3-mercaptopropionic acid (MPA)-AuNPs

MPA-AuNPs were synthesized by preparing citrate stabilized AuNPs as a first step and using a ligand exchange reaction to create the desired AuNPs, which is described elsewhere.[27] The diameter of the particles was found to be 4.8 ± 1.1 nm by transmission electron microscopy (TEM). The MPA-capping is pH-sensitive and has a pKa of 4.3.[28]

3. Preparation of brush/AuNP composite materials

PMETAC brushes were incubated for 6 h into the AuNP suspension to achieve brush/AuNP composites. The AuNP suspension had a concentration of 0.16 mg/ml.[27] The pH was adjusted to pH 4 and 8, respectively. Here, two different buffer systems (formic acid/KOH and TRIS/HCl) were used to adjust the incubation medium to pH 4 and pH 8 with the same ionic strength of around 0.05M. The detailed preparation of both buffer systems is described elsewhere.[27] After incubation, the samples were taken out, sonicated in Milli-Q water for 1 min, and dried under a nitrogen stream.

C. Instruments and measurement procedures

1. Transmission Electron Microscopy (TEM)

TEM measurements were performed on a FEI Tecnai G^2 20 S-TWIN (FEI, Hillsboro, OR, USA). TEM copper grids with a carbon film were used (200 mesh, Science Service, Munich, Germany). Electric charge was removed by glow discharge for 15 s. Subsequently, 5 μl of the sample solution were deposited onto the grids. After 1 min incubation, the excess liquid and AuNPs were blotted with a filter paper. The grids were then dried at room temperature and placed inside the TEM. The images were analyzed using ImageJ. The size of AuNPs was determined by averaging 200 particles.

2. Ellipsometry

The ellipsometric measurements were carried out with a polarizer-compensator sample analyzer (PCSA) ellipsometer (Optrel GbR, Sinzing, Germany) at a wavelength of 632.8 nm in the null ellipsometry mode. The measurements were carried

TABLE I. One-layer-model for fitting polymer brushes on a silicon wafer against air or water. Parameters are refractive index n, absorption coefficient k, and the thickness of the layer, respectively. Arrays with an infinity symbol imply bulk properties with quasi-infinity thickness. Arrays with "fit" indicate the fitting parameters.

Layer	N	k	Thickness (nm)
Air	1	0	∞
Brush	Fit	0	Fit
SiO_x	1.50	0	1.50
Si	3.885	−0.020	∞

out at an angle of incidence of 70° under ambient conditions (≈30% RH). The data were fitted with Elli v3.1 (Optrel, Sinzing, Germany) based on a one-layer-model for the polymer brushes shown in Table I.

3. Neutron Reflectometry (NR) measurements and reflectivity analysis

NR measurements were carried out at the reflectometer V6 at Helmholtz-Zentrum Berlin (Berlin, Germany).[29] All measurements were carried out using solid/liquid cells at a controlled temperature of $T = 25\,°C$. After passing through the silicon block, the monochromatic incident beam with wavelength $\lambda = 4.66$ Å hits the solid/liquid interface at a variable incident angle θ and is reflected at the same angle. The reflectivity R, e.g., the intensity ratio between reflected and incident beams is recorded as a function of $q_z = (4\pi/\lambda)\sin\theta$, the scattering vector component perpendicular to the interface. The value of q_z ranged from 0.005 Å^{-1} to 0.10 Å^{-1}. The wavelength resolution was $\delta\lambda/\lambda = 2\%$, resulting in a finite q_z-resolution, which was taken into consideration for the data analysis by convolution with Gaussian functions.[30–32] The measuring time per run varied between 12 h and 18 h.

The reflectivity curves $R(q_z)$ depend on the interfacial scattering length density (SLD) profiles $\rho(z)$, where z denotes the position on the axis perpendicular to the surface plane. The SLD profiles depend on the interfacial volume fraction profiles $\Phi_i(z)$ of all chemical components i with known SLD ρ_i,

$$\rho(z) = \sum_i \Phi_i(z) \cdot \rho_i. \tag{1}$$

The profiles are described with parameter-based analytical functions,[31,32] as specified in Sec. III. The SLD of water, ρ_W, is different for H_2O ($\rho_W = -0.56 \times 10^{-6}$ Å^{-2}), 4-matched water 4MW ($\rho_W = 4.00 \times 10^{-6}$ Å^{-2}), and D_2O ($\rho_W = 6.36 \times 10^{-6}$ Å^{-2}). To compute theoretical reflectivity curves for comparison with the experimental ones, the $\rho(z)$ profiles were discretized into hundreds of thin slabs of 2 Å thickness and constant SLD. The reflectivity curves were then calculated by the application of Fresnel's reflection laws at each slab/slab interface and the phase-correct summation using the iterative procedure of Parratt.[33] In the last step, the model parameters describing the volume fraction profiles were varied until the best simultaneous agreement (characterized by the minimal chi-square deviation) was reached simultaneously with the experimental reflectivity curves measured in all water contrasts. Roughness parameters were restrained to values above 2 Å for all interfaces associated with the solid substrate and to values above 5 Å for all other interfaces. The fitting program was implemented in the IDL programming language (IDL 8.6, www.harrisgeospatial.com).

III. RESULTS

To get a full understanding about AuNPs adsorption onto/into the PMETAC brush at different pH, one needs information about the assembly of AuNP in suspension before the incubation of PMETAC brushes. Therefore, Sec. III A deals with the characterization of AuNP suspensions. Here, TEM measurements were carried out of AuNP suspensions at different pH. Section III B addresses the internal structure of a PMETAC brush before and after the incubation in AuNP suspension to form PMETAC/AuNP composite materials. Neat PMETAC brush and PMETAC brushes after incubation at pH 4 and at pH 8 were measured by NR against different water contrasts.

A. AuNP suspension at different pH

The particle-particle interaction at different pH was investigated by mixing AuNP stock suspension with buffer solution with a pH ranging from 4 to 8. TEM measurements were performed to characterize the particle behavior and are shown in Fig. 1. AuNPs at pH 4 form compact aggregates. At pH 6, network-like aggregation occurs between AuNPs, while at pH 8, a stable suspension of individual AuNPs is observed. Clear differences in the AuNP bulk behavior can be observed, which likely has an effect also on the AuNP assembly in the PMETAC brush. Although an influence of the drying step on the particle distribution (see Sec. II C) cannot be fully excluded, the strong impact of pH on the colloidal stability, as seen qualitatively in the TEM images, can be considered a robust result.

B. Neutron Reflectometry (NR) measurements

NR is sensitive to the distribution of AuNPs within the brush because the SLDs of PMETAC and AuNPs are very different:[34,35] $\rho_{PME} \approx 0.9 \times 10^{-6}$ Å^{-2} and $\rho_{AuNP} \approx 3.6 \times 10^{-6}$ Å^{-2}, respectively. ρ_{AuNP} can be estimated *a priori* by assuming a spherical shape uniform face centered cubic (fcc) structure[36] of Au and a uniform coverage of MPA around the AuNP (see Fig. 2).

A diameter of 4.8 nm for the AuNP core was obtained from TEM (see Sec. II C). The length of MPA as a coating was estimated as 0.68 nm from theoretically calculations.[37] The SLD of the AuNPs, ρ_{AuNP}, was calculated by

$$\rho_{AuNP} = \frac{V_{Au} \cdot \rho_{Au} + V_{MPA} \cdot \rho_{MPA}}{V_{Au} + V_{MPA}}, \tag{2}$$

with $\rho_{Au} = 4.66 \times 10^{-6}$ Å^{-2} and $\rho_{MPA} = 1.37 \times 10^{-6}$ Å^{-2} (calculation was done by dividing the sum of the scattering length contribution from all atoms within the molecule with its solvent-inaccessible molecular volume). V_{Au} and V_{MPA} denote

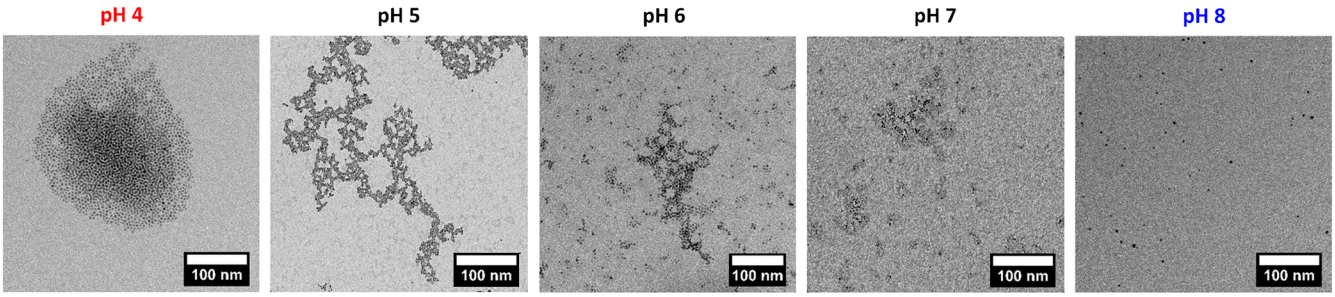

FIG. 1. AuNPs dispersed in buffer solution with different pH ranging from 4 to 8 and measured by TEM.

the volume of the gold and the MPA-capping, respectively. A SLD of $\rho_{\mathrm{AuNP}} = 3.58 \times 10^{-6}$ Å^{-2} was obtained.

With the help of water contrast variation, the interfacial distributions of PMETAC, $\Phi_{PME}(z)$, and of the AuNPs, $\Phi_{\mathrm{AuNP}}(z)$, can be unambiguously disentangled (see Fig. 3). Namely, the AuNPs are nearly invisible in the 4MW contrast so that the corresponding reflectivity curve is dominated by the brush profile. In the H_2O contrast, on the other hand, the reflectivity curve is dominated by the AuNP distribution. Finally, in the D_2O contrast, both components contribute. The neat brushes as well as the brushes after adsorption of AuNPs at pH 4 and at pH 8 were characterized against all three contrasts.

1. Characterization of a neat PMETAC brush

Figure 4(a) shows the experimental reflectivity curves obtained with D_2O, 4MW, and H_2O contrasts. The solid lines represent the simulated reflectivity curves corresponding to the best-matching parameters in the common model [Figs. 4(b) and 4(c)], which is based on the volume fraction profiles, $\Phi_i(z)$, of silicon ("Si"), silicon oxide ("SiO_2"), initiator ("ini"), PMETAC ("PME"), and water ("W"). This roughness-free representation in Fig. 4(b) merely serves for an illustration of the parametric mathematical model. The associated SLD profile $\rho(z)$ follows as

$$\rho(z) = \Phi_{\mathrm{Si}}(z) \cdot \rho_{\mathrm{Si}} + \Phi_{\mathrm{SiO_2}}(z) \cdot \rho_{\mathrm{SiO_2}} + \Phi_{ini}(z) \cdot \rho_{ini} + \Phi_{PME}(z) \cdot \rho_{PME} + \Phi_W(z) \cdot \rho_W, \quad (3)$$

where the position $z = 0$ is defined as the interface between the initiator layer and the aqueous region accommodating the PMETAC brush. $\Phi_{\mathrm{Si}}(z)$ is modeled as a semi-infinite continuum with fixed SLD $\rho_{\mathrm{Si}} = 2.07 \times 10^{-6}$ Å^{-2}, which is the literature value. $\Phi_{\mathrm{SiO_2}}(z)$ and $\Phi_{ini}(z)$ are represented as homogeneous slabs with adjustable thicknesses $d\mathrm{SiO_2}$ and $d$ini, respectively, and adjustable roughnesses between the layers, characterized by roughness parameters $\delta_{\mathrm{Si/SiO_2}}$, $\delta_{\mathrm{SiO_2}/ini}$, and $\delta_{ini/PME}$. The SLD of SiO_2 is fixed at the literature value $\rho_{\mathrm{Si}} = 3.47 \times 10^{-6}$ Å^{-2}. However, earlier studies showed that the SiO_2 can incorporate a finite amount of solvent, which is characterized by an adjustable parameter $\Phi^{\mathrm{SiO_2}}_{solvent}$.[30–32,38] The SLD of the initiator layer, ρ_{ini}, was set as a free parameter. For convenience and in lack of a reliable estimate, its solvent content was neglected. Initially, the SLD of PMETAC, ρ_{PME}, was a free parameter. According to the recent work of Micciulla *et al.*,[30] the PMETAC volume fraction profile Φ_{PME} was modeled as a two-region distribution [Fig. 4(b)],

$$\Phi_{PME}(z) = \Phi^{in}_{PME}(z) + \Phi^{out}_{PME}(z). \quad (4)$$

The inner region $\Phi^{in}_{PME}(z)$ corresponds to the dense brush region near the grafting surface, which is represented by a homogeneous slab characterized by its thickness d^{in}_{PME} and its maximal volume fraction Φ^0_{PME}. The outer region $\Phi^{out}_{PME}(z)$ describes the dilute brush periphery, represented by a stretched exponential function

$$\Phi^{out}_{PME}(z) = I_{in/out}(z) \cdot \Phi^0_{PME} \cdot \exp(-(\frac{z}{\Lambda})^n), \quad (5)$$

where $I_{in/out}(z)$ accounts for the gradual transition between the dense brush region and the dilute brush region in the form of an error function characterized by the roughness parameter $\delta^{in/out}_{PMETAC}$. Λ and n denote the decay length of the brush volume fraction and the stretching exponent, respectively. Finally, the water volume fraction profile follows from the requirement that the sum of all volume fractions equals unity at each z-position,

$$\sum_i \Phi_i(z) \equiv 1, \quad (6)$$

which is shown in Figs. 4(c), 5(c), and 6(c) as dashed lines. Figure 4(c) shows the volume fraction profile according to the best-matching model parameters, corresponding to the fits in Fig. 4(a). The two-region model is sufficient to describe the neat PMETAC brush. The volume fraction profiles also constitute the basis for the schematic illustration in Fig. 4(d). The inner region of the PMETAC brush, with thickness $d^{in}_{PME} = 110 \pm 10$ Å, comprises most of the total polymer amount. The outer region exhibits a characteristic decay length of $\Lambda = 330 \pm 20$ Å and a stretching exponent of $n = 1.8 \pm 0.2$.

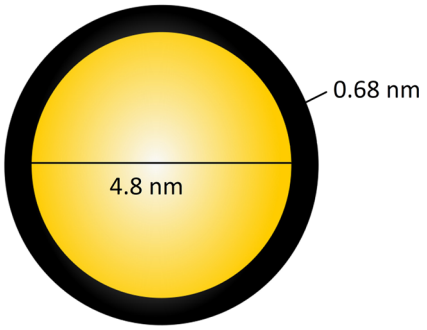

FIG. 2. Schematic illustration of AuNPs coated with MPA.

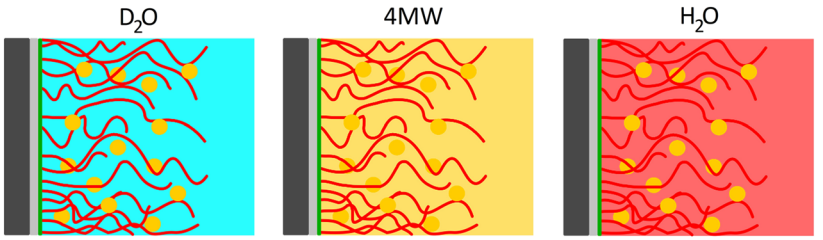

FIG. 3. Schematic illustration of a PMETAC/AuNP composite in different water contrasts. Measuring the composite against D_2O (left) offers substantial contrast to both the PMETAC brush and the AuNPs. In 4MW (middle), the AuNP SLD is nearly matched out by the solvent so that the measurement is mostly sensitive to the brush profile. In H_2O (right), the SLD contrast with the brush is weak and the measurement is mostly sensitive to the AuNP distribution.

The brush amount per surface area in terms of an equivalent thickness D_{PME} is conveniently obtained by integration,

$$D_{PME} = \int_{-\infty}^{+\infty} \Phi_{PME}(z)dz. \tag{7}$$

D_{PME} corresponds to the thickness of a layer of 100% PMETAC (without any water or free voids). We obtain D_{PME} = 140 Å ± 5 Å, which is thinner than the thickness delli = 212 ± 13 Å measured by ellipsometry under ambient conditions (≈30% RH). The deviation can be attributed to the residual water content in the brush under ambient conditions and to differences between the volumes relevant for the calculation of SLD (partial molecular volume) and refractive index (inverse density). According to Löhmann *et al.*,[39] a PMETAC brush prepared with the same protocol contains up to 20 vol. % water in the range between 30 and 50% RH.

The SLD of the initiator layer is obtained as $\rho_{ini} \approx 0.95 \times 10^{-6}$ Å^{-2} and that of PMETAC is obtained as $\rho_{PME} \approx 0.84 \times 10^{-6}$ Å^{-2}. The obtained SLDs agree well with the theoretical calculated value for $\rho_{ini} = 1.06 \times 10^{-6}$ Å^{-2} (calculated by dividing the sum of all atomic scattering lengths by the solvent-inaccessible volume) and the theoretical estimate of $\rho_{PME} = 0.88 \times 10^{-6}$ Å^{-2} based on a the METAC monomer volume of VMETAC = 262 Å.[3,40] Furthermore, an experimental value of $\rho_{PME} = 0.82 \times 10^{-6}$ Å^{-2} was reported by Löhmann *et al.*[39] and is in line with our results. While several studies have reported that polymer and polyelectrolyte brushes tend to degraft when exposed to good solvents,[41–43] no significant degrafting occurred in the present study. In fact, it would have been difficult to commonly model neutron reflectivity curves recorded sequentially in three water contrasts if significant degrafting had occurred on the time scale of the experiments. The reason why degrafting was not an issue in the present work may be that it is less pronounced for thin brushes formed by comparatively short chains, as was proposed earlier.[44]

2. Characterization of a PMETAC brush after incubation in AuNP suspension at pH 4

Analysis of the reflectivity curves after AuNP adsorption requires the extension of the volume fraction model by the AuNP profile $\Phi_{\mathrm{AuNP}}(z)$,

$$\rho(z) = \Phi_{\mathrm{Si}}(z) \cdot \rho_{\mathrm{Si}} + \Phi_{\mathrm{SiO_2}}(z) \cdot \rho_{\mathrm{SiO_2}} + \Phi_{ini}(z) \cdot \rho_{ini} + \Phi_{PME}(z) \cdot \rho_{PME} + \Phi_{\mathrm{AuNP}}(z) \cdot \rho_{\mathrm{AuNP}} + \Phi_W(z) \cdot \rho_W. \tag{8}$$

Here, ρ_{ini} and ρ_{PME} were fixed to the values obtained in the fits of the neat brush (see Sec. III B 1), while ρ_{AuNP} was set as a free parameter. $\Phi_{\mathrm{AuNP}}(z)$ is described as a unimodal distribution in the form of one rough slab, characterized by its respective center position (z^{AuNP}), thickness (d^{AuNP}), maximal volume fraction (Φ_0^{AuNP}), and roughness parameter on both sides of the slab ($\delta_{\mathrm{AuNP}}^{left}$, $\delta_{\mathrm{AuNP}}^{right}$). Concerning the PMETAC profile after AuNP adsorption, the two-region description according to Eq. (4) (see Sec. III B 1) was no longer sufficient, reflecting that Φ_{PME} is significantly perturbed by the AuNP adsorption. Instead, a three-region description was employed [see Fig. 5(b)], comprising two adjacent rough slabs and a stretched exponential function representing the dilute brush periphery in analogy to Eq. (5). This slightly more complex description was found to be versatile enough to capture the perturbation of the brush profile upon AuNP adsorption.

Figure 5(a) shows the experimental reflectivity curves against D_2O, 4MW, and H_2O obtained after adsorption of AuNP at pH 4. The solid lines in 5(a) again represent the simulated reflectivity curves corresponding to the best-matching parameters in the common model [Figs. 5(b) and 5(c)].

The volume fraction profile shows that the PMETAC brush gets stretched after the incubation. The inner region of the PMETAC brush, with thickness d_{PME}^{in} = 600 ± 30 Å, comprises most of the total polymer amount. The outer region exhibits a characteristic decay length of Λ = 600 ± 40 Å and a stretching exponent of n = 3 ± 0.5. It indicates, that the peripheral edge of the brush becomes somewhat sharper with respect to the neat PMETAC brush. The AuNPs are not homogeneously distributed over the brush. Instead, they are rather confined near the brush periphery and apparently unable to fully penetrate the brush. One can see this from $\Phi_W(z)$ that the AuNPs replace water at the position in which they are confined.

Previous studies[23,27] have demonstrated that the AuNPs are rather uncharged at pH 4 and therefore tend to aggregate. XRR measurements qualitatively suggested that these aggregates are preferably adsorbed to the brush periphery.[23,27] The aggregates were detected by AFM and TEM images. A schematic illustration of the AuNP distribution is drawn in Fig. 5(d).

The maximal volume fraction of AuNPs attached to the brush is around 18 vol. %, which was also found by XRR measurements.[23] The number of adsorbed AuNPs per surface area can be extracted from the volume fraction profile according to

$$\sigma_{\mathrm{AuNP}} = \frac{1}{V_{\mathrm{AuNP}}} \int_{-\infty}^{+\infty} \Phi_{\mathrm{AuNP}}(z)dz, \tag{9}$$

where $V_{\mathrm{AuNP}} \approx 58$ nm^3 is the average AuNP volume. With that, we obtain $\sigma_{\mathrm{AuNP}} \approx 0.07$ nm^{-2}, corresponding to one AuNP per

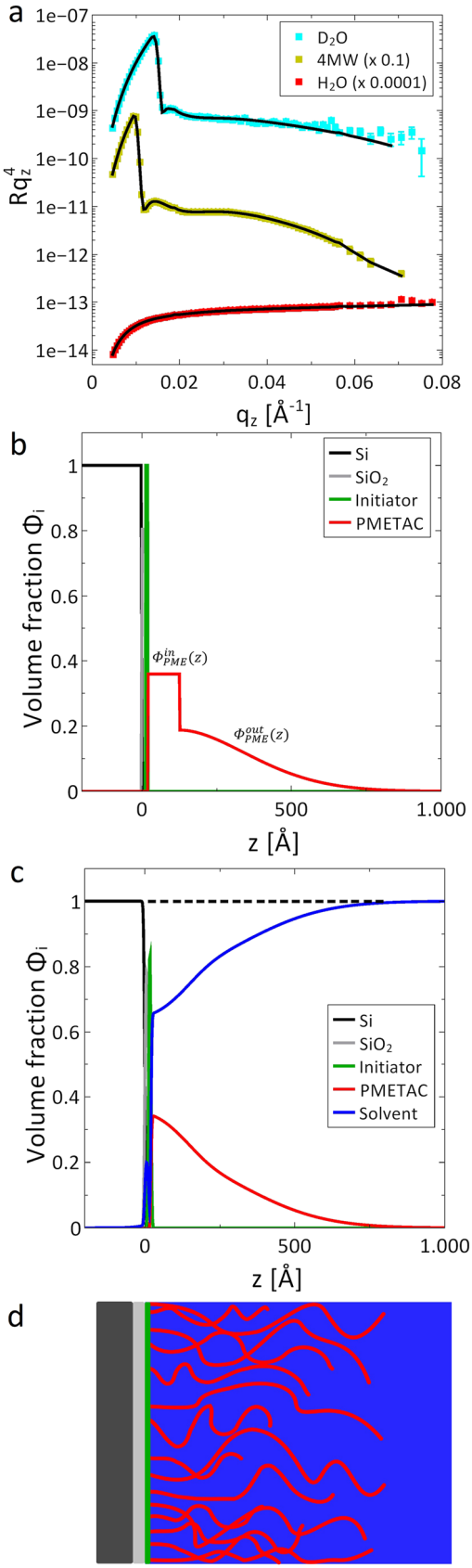

FIG. 4. (a) Reflectivity curves and best fits for a neat brush. (b) Schematic illustration of the theoretical model used to interpret the experimental reflectivity curves. This roughness-free representation merely serves for an illustration of the parametric mathematical model. (c) Best-matching profiles obtained in the fits [solid lines in panel (a), the reflectivity curves]. The dashed line indicates that the sum of all volume fractions is one. (d) Schematic representation of a neat PMETAC brush in an aqueous solvent.

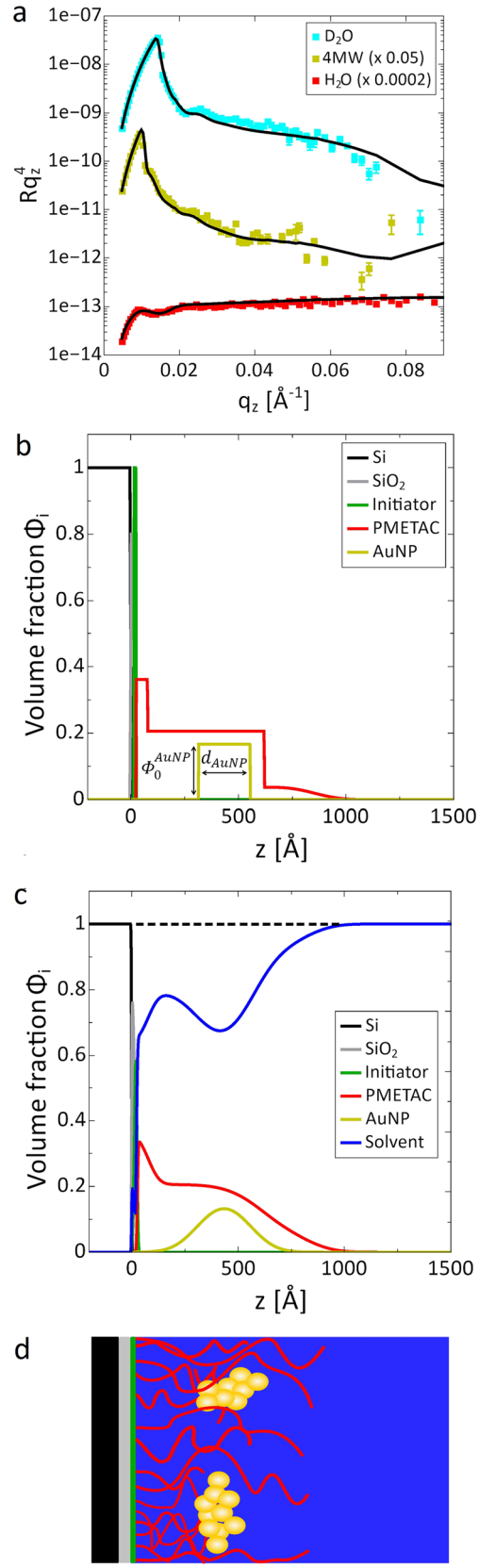

FIG. 5. (a) Reflectivity curves and best fits for a PMETAC/AuNP composite at pH 4. (b) Schematic illustration of the theoretical model used to interpret the experimental reflectivity curves. This roughness-free representation merely serves for an illustration of the parametric mathematical model. (c) Best-matching profiles obtained in the fits [solid lines in panel (a), the reflectivity curves]. The dashed line indicates that the sum of all volume fractions is one. (d) Schematic representation of a PMETAC/AuNP composite at pH 4 in an aqueous solvent.

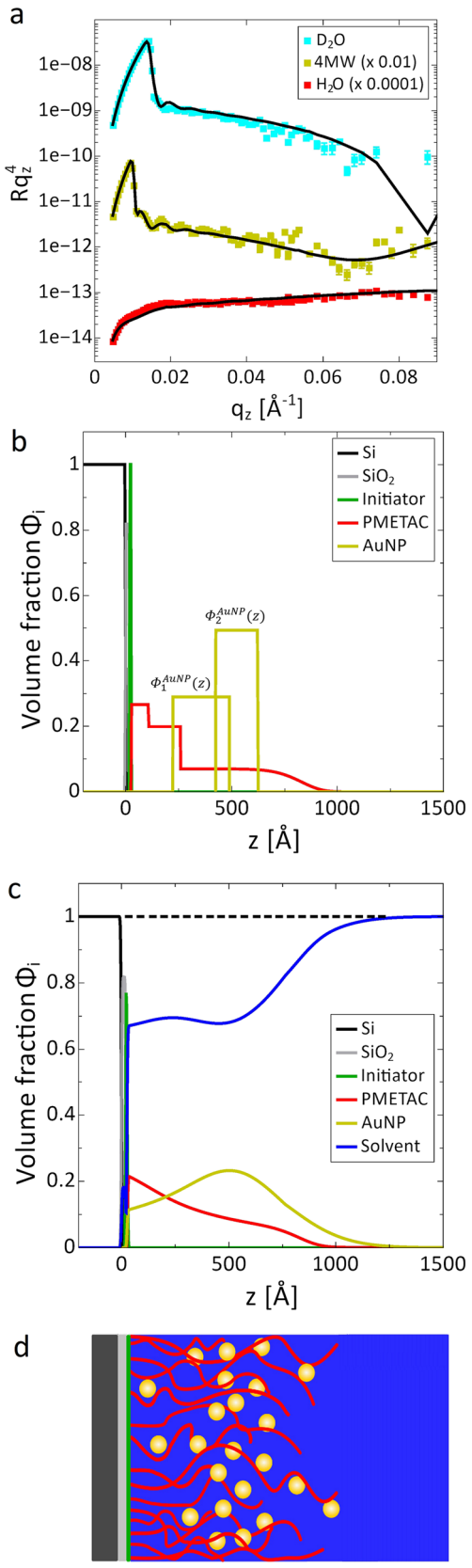

FIG. 6. (a) Reflectivity curves and best fits for a PMETAC/AuNP composite at pH 8. (b) Schematic illustration of the theoretical model used to interpret the experimental reflectivity curves. This roughness-free representation merely serves for an illustration of the parametric mathematical model. (c) Best-matching profiles obtained in the fits [solid lines in panel (a), the reflectivity curves]. The dashed line indicates that the sum of all volume fractions is one. (d) Schematic representation of a PMETAC/AuNP composite at pH 8 in an aqueous solvent.

14 nm^{-2}. The best-matching SLD of the AuNPs is obtained as $\rho_{\mathrm{AuNP}} = 3.8 \times 10^{-6}$ Å^{-2}, which is in good agreement to our *a priori* estimate of $\rho_{\mathrm{AuNP}} = 3.58 \times 10^{-6}$ Å^{-2}.

3. Characterization of a PMETAC brush after incubation in AuNP suspension at pH 8

For the characterization of a PMETAC brush after incubation in AuNP suspension at pH 8, the same three-region description was used for the PMETAC brush in the PMETAC/AuNP composite, while for $\Phi_{\mathrm{AuNP}}(z)$, a unimodal description was not sufficient. Instead, a bimodial distribution, represented by two rough slabs, was employed [see Fig. 6(b)],

$$\Phi_{\mathrm{AuNP}}(z) = \Phi_1^{\mathrm{AuNP}}(z) + \Phi_2^{\mathrm{AuNP}}(z). \tag{10}$$

The two rough slabs are characterized by their respective center positions (z_1^{AuNP} and z_2^{AuNP}), thicknesses (d_1^{AuNP} and d_2^{AuNP}), maximal volume fractions (Φ_0^{AuNP1} and Φ_0^{AuNP2}), and roughness parameters on both sides ($\delta_{\mathrm{AuNP1}}^{left}$, $\delta_{\mathrm{AuNP1}}^{right}$ and $\delta_{\mathrm{AuNP2}}^{left}$, $\delta_{\mathrm{AuNP2}}^{right}$). Earlier results[23,27] showed qualitatively that at pH 8, the AuNPs are well dispersed in suspension because they are highly negatively charged and therefore electrostatically stabilized as individual particles. The reflectivity data and the description of the AuNP distribution are shown in Fig. 6(a). The solid lines show the best fits. The experimental data could be well described by the bimodial description. Figure 6(c) shows the volume fraction profiles according to the best-matching model parameters. Corresponding to the volume fraction profiles, a schematic illustration of the AuNP distribution is drawn in Fig. 6(d).

The SLD of AuNPs was found to be $\rho_{\mathrm{AuNP}} = 3.9 \times 10^{-6}$ Å^{-2}, which is in good agreement with the value found for the AuNPs attached to the brush after the incubation at pH 4 and to our *a priori* estimate. The good agreement concerning ρ_{AuNP} obtained for the two different data sets (PMETAC/AuNP composites at pH 4 and at pH 8) can be understood as an indication of the robustness of the analysis.

The volume fraction profiles show that the PMETAC brush swells up to ≈200 Å more in comparison to the neat PMETAC brush due to the AuNP incorporation, while water is replaced by the AuNPs. The inner region of the PMETAC brush, with thickness $d_{PME}^{in} = 230 \pm 20$ Å, comprises most of the total polymer amount. The outer region exhibits a characteristic decay length of $\Lambda = 600 \pm 30$ Å and a stretching exponent of $n = 7 \pm 2$, meaning that the brush periphery is nearly box-like with a low PMETAC fraction. AuNPs are distributed over the entire brush but not in a homogeneous manner. It was found that the relative amount of AuNPs in the dilute PMETAC region is higher with almost 25 vol. % than in the dense PMETAC region toward the substrate with 15 vol. %. The number of adsorbed AuNPs per surface area in total is obtained as $\sigma_{\mathrm{AuNP}} \approx 0.18$ nm^{-2} [see Eq. (9)], corresponding to one AuNP per 6 nm^{-2}.

IV. DISCUSSION

A. AuNP formation in suspension at different pH

MPA-capped AuNPs are pH-sensitive since the capping bears a carboxylic group with a pKa of 4.3.[28] TEM

images in Fig. 1 reveal that decreasing the pH decreases the interparticle distance due to protonation of the carboxylic acid group on the surface, resulting in the reduction of electrostatic repulsion. At pH 4, AuNPs aggregate but still have deprotonated carboxylic acid groups and the ability to interact with the positively charged PMETAC brush in order to form PMETAC/AuNP composites. At pH 8, on the other hand, AuNPs are electrostatically stabilized and do not agglomerate. The carboxylic acid groups of the MPA capping are highly deprotonated at pH 8, and a favorable electrostatic interaction between AuNPs and the PMETAC brush is expected. Previous studies have shown that particle-particle interactions in the bulk aqueous suspension are an important aspect also for the particle adsorption into the PMETAC brush.[23,27]

B. Internal characterization of neat PMETAC brush and PMETAC/AuNP composites in different water contrasts

Earlier NR experiments[23] with one single water contrast (D_2O) and a standard box-model description of the SLD profile already yielded qualitative insights into the PMETAC brush and composite structures. However, it had not been possible to extract the amounts and SLDs of the individual components. In the present work, the combination of multiple water contrasts with a self-consistent analysis based on continuous volume fraction profiles make it possible to extract the amounts, SLDs, and distributions of all chemical components and, with that provides comprehensive information on the composites internal structure.

The volume fraction profile of a neat PMETAC brush [Fig. 4(c)] shows that the brush is highly hydrated. The observed high water content can be attributed to the osmotic pressure of the counterions inside the brush.[45] A stretching exponent of $n = 1.8 \pm 0.2$ reflects a moderate polydispersity, compared to $n = 0.9 \pm 0.2$ found in the work of Micciulla *et al.*[30] The lower polydispersity in the present paper can be attributed to a slow polymerization during PMETAC synthesis.[46,47]

AuNPs do not fully penetrate the brush after incubation of a PMETAC brush in AuNP suspension at pH 4 since they are aggregated and too bulky to penetrate the brush. Instead, they mostly adsorb at the brush periphery. As already pointed out further above, AuNPs at pH 4 still have deprotonated carboxylic acid groups and thus the tendency to interact with the positively charged PMETAC brush. The associated release of counterions is normally expected to result in the reduction of the osmotic pressure inside the brush and, in turn, in a more compact brush conformation. For similar reasons, polyelectrolyte brushes assume more compact conformations in the presence of salt.[26,48] In contrast to this expectation, the adsorption of AuNPs leads to a more extended brush conformation [see Fig. 5(c)]. This finding is robust and must be attributed to volumetric effects of the AuNPs themselves: They occupy up to almost 20 vol. % [see Fig. 5(c)] and therefore replace the PMETAC further away from the solid surface. The obtained volume fraction profiles further exclude an alternative swelling mechanism based on the enhanced water incorporation or an increase in osmotic pressure along with the particles.

At pH 8, AuNP adsorption occurs into the entire brush, as evidenced from the broad AuNP volume fraction profile in Fig. 6(c). The overall AuNP amount per unit area ($\sigma_{\mathrm{AuNP}} \approx 0.18\ \mathrm{nm}^{-2}$) is 2.6 times larger than at pH 4 ($\sigma_{\mathrm{AuNP}} \approx 0.07\ \mathrm{nm}^{-2}$). The associated much stronger volumetric effect is manifested also in the even more extended brush conformation observed at pH 8 [see Fig. 6(c)]. We cannot exclude, however, that a part of the effect results also from the mutual repulsion between brush-adsorbed AuNPs. When comparing the different AuNP distributions at pH 4 and pH 8, it is rewarding to consider the osmotic penalty, $F_{osm} = N \cdot V_{\mathrm{AuNP}} \cdot \Pi_{osm}$, associated with the insertion into the brush of an aggregate of N particles versus that of an individual AuNP ($N = 1$). Here, Π_{osm} denotes the osmotic pressure inside the brush, which scales approximately linearly with the PMETAC volume fraction. It is seen that this penalty is much larger for the aggregates than for the individual particles, which rationalizes the impermeability of the dense brush region for the aggregates (at pH 4) but not for the individual AuNPs (at pH 8). In this context, it should be noted that the distribution of AuNPs is not homogeneous. PMETAC brushes possess two regions, a dense inner region and a dilute outer region, which are characteristic for polyelectrolyte brushes created via the grafting from approach.[49,50] More AuNPs are attached to the dilute brush region while less AuNPs can penetrate the dense brush region. This trend can also be interpreted as a manifestation of this osmotic penalty. The exact distribution of particles within the brush as well as the exact overall adsorbed particle amount depends on a subtle interplay of various physical mechanisms promoting and suppressing particle adsorption into polyelectrolyte brushes. These mechanisms have been discussed in the literature, are partially antagonistic, and include (i) favorable interactions between polymers and particles,[51] which at pH 8 are at least partially of electrostatic nature, (ii) release of counterions upon particle insertion, (iii) the electrostatic self-energy of charged particles which reduces upon adsorption due to the high ion concentration inside the brush,[52] and (iv) the osmotic penalty mentioned above, which consists of a contribution from the polymers[51,53] and for polyelectrolyte brushes additionally of the counter-ion contribution.[45] In view of this complexity and without reliable estimates for the individual contributions at hand, we refrain from a quantitative theoretical interpretation of the obtained brush and AuNP distributions.

V. CONCLUSION

We have investigated the internal structure of solid-grafted PMETAC polyelectrolyte brushes in an aqueous environment before and after the adsorption of surface-modified AuNPs at two different pH conditions. In order to determine the interfacial distributions of the brush and the adsorbed particles, we have carried out NR in multiple water contrasts to systematically hide one of the components in each measurement so that the distribution of the other one is obtained unambiguously. The reflectivity data were analyzed with a self-consistent model based on analytically parameterized volume fraction profiles. This procedure did not only enable the determination of the SLDs of brush and particles but also provided structural

information of much greater detail than what had been obtained in previous reflectivity studies using standard approaches.[23]

Our measurements revealed that AuNPs adsorbing at pH 4 in the form of aggregates are unable to fully penetrate the brush, despite significantly favorable electrostatic interactions. Adsorption instead occurs mostly at the brush periphery and is accompanied by a significant stretching of the brush due to the particles volumetric effect. At pH 8, AuNPs are highly charged, adsorb as individual particles into the entire brush at very high overall numbers, and induce an even more pronounced brush extension. The insights gained in the present work provide valuable information for the future design of PMETAC/AuNP composites for stimuli-responsive colorimetric sensors.

ACKNOWLEDGMENTS

The authors gratefully thank Maren Lehmann and Marcus Witt for TEM measurements and Joachim Dzubiella for insightful comments. TEM experiments were carried out at the electron microscope of the Joint Laboratory for Structural Research (JLSR) of Helmholtz-Zentrum Berlin für Materialien und Energie (HZB), Humboldt-Universität zu Berlin, (HU) and Technische Universität Berlin (TU). Furthermore, we thank the Helmholtz-Zentrum Berlin for the allocation of neutron beamtime. Financial support was granted by the German Research Foundation (DFG) via the International Research Training Group (IRTG) 1524. Additional financial support came from TU Darmstadt. E.S. acknowledges financial support by the Max Planck Society and from an Emmy-Noether Grant (No. SCHN 1396/1) by the German Research Foundation (DFG).

[1] H. Hu, M. Gopinadhand, and C. O. Osuji, Soft Matter **10**, 3867 (2014).
[2] H. Löwen, J. Phys.: Condens. Matter **13**, R415 (2001).
[3] W.-L. Chen, R. Cordero, H. Tran, and C. K. Ober, Macromolecules **50**, 4089 (2017).
[4] O. Azzaroni, J. Polym. Sci., Part A: Polym. Chem. **50**, 3225 (2012).
[5] T. J. Murdoch, B. A. Humphreys, J. D. Willot, S. W. Prescott, A. Nelson, G. B. Webber, and E. J. Wanless, J. Colloid Interface Sci. **490**, 869 (2017).
[6] T. Zhou, L. Han, D. Barbash, and C. Y. Li, Nat. Commun. **7**, 1 (2016).
[7] J. Parvole, J.-P. Montfort, G. Reiter, O. Borisov, and L. Billon, Polymer **47**, 972 (2006).
[8] M. Iacono, D. Connolly, and A. Heise, RSC Adv. **7**, 19976 (2017).
[9] R. A. E. Wright, K. Wang, J. Qu, and B. Zhao, Angew. Chem., Int. Ed. **55**, 8656 (2016).
[10] J. P. Gann and M. Yan, Langmuir **24**, 5319 (2008).
[11] Q. Chen, Langmuir **30**, 8119 (2014).
[12] S. P. Adiga and D. W. Brenner, J. Funct. Biomater. **3**, 239 (2012).
[13] G. Emilsson, K. Xiong, Y. Sakiyama, B. Malekian, V. A. Gagner, R. L. Schoch, R. Y. H. Lim, and A. B. Dahlin, Nanoscale **10**, 4663 (2018).
[14] I. Tokareva, S. Minko, J. H. Fendler, and E. Hutter, J. Am. Chem. Soc. **126**, 15950 (2004).
[15] L. I. Klushin, A. M. Skvortsov, A. A. Polotsky, S. Qi, and F. Schmid, Phys. Rev. Lett. **113**, 068303 (2014).
[16] A. K. Patel, P. S. Sharma, and B. B. Prasad, Mater. Sci. Eng.: C **29**, 1545 (2009).
[17] T. Chen, R. Ferris, J. Zhang, R. Drucker, and S. Zauscher, Prog. Polym. Sci. **35**, 94 (2010).
[18] M. König, E. Bittrich, U. König, B. L. Rajeev, M. Müller, K. J. Eichhorn, S. Thomas, M. Stamm, and P. Uhlmann, Colloids Surf., B **146**, 737 (2016).
[19] V. Amendola, R. Pilot, M. Frasconi, O. M. Marago, and M. A. Iati, J. Phys.: Condens. Matter **29**, 203002 (2017).
[20] S. K. Ghosh and T. Pal, Chem. Rev. **107**, 4797 (2007).
[21] N. Fortin and H.-A. Klok, ACS Appl. Mater. Interfaces **7**, 4631 (2015).
[22] A. R. Ferhan, L. Guo, X. Zhou, P. Chen, S. Hong, and D.-H. Kim, Anal. Chem. **85**, 4094 (2013).
[23] D. Kesal, S. Christau, M. Trapp, P. Krause, and R. von Klitzing, Phys. Chem. Chem. Phys. **19**, 30636 (2017).
[24] D. Boyaciyan, P. Krause, and R. von Klitzing, Soft Matter **14**, 4029 (2018).
[25] P. Laurent, G. Souharce, J. Duchet-Rumeau, D. Portinha, and A. Charlot, Soft Matter **8**(3), 715 (2012).
[26] S. Moya, O. Azzaroni, T. Kelby, E. Donath, and W. Huck, J. Phys. Chem. B **111**, 7034 (2007).
[27] D. Kesal, S. Christau, P. Krause, T. Möller, and R. von Klitzing, Polymers **8**(4), 134 (2016).
[28] F. Reincke, W. K. Kegel, H. Zhang, M. Nolte, D. Wang, D. Vanmaekelbergh, and H. Möhwald, Phys. Chem. Chem. Phys. **8**, 3828 (2006).
[29] M. Trapp, J. Large-Scale Res. Facil. **3**, A114 (2017).
[30] S. Micciulla, Y. Gerelli, R. A. Campbell, and E. Schneck, Langmuir **34**, 789 (2018).
[31] E. Schneck, A. Schollier, A. Halperin, M. Moulin, and M. Härtlein, Langmuir **29**, 14178 (2013).
[32] E. Schneck, I. Berts, A. Halperin, J. Daillant, and G. Fragneto, Biomaterials **46**, 95 (2015).
[33] L. G. Parratt, Phys. Rev. **95**, 359 (1954).
[34] I. E. Dunlop, R. K. Thomas, S. Titmus, V. Osborne, S. Edmondson, W. T. S. Huck, and J. Klein, Langmuir **28**, 3187 (2012).
[35] N. Krasteva, R. Krustev, A. Yasuda, and T. Vossmeyer, Langmuir **19**, 7754 (2003).
[36] X. Liu, M. Atwater, J. Wang, and Q. Huo, Colloids Surf., B **58**, 3 (2007).
[37] H. Hinterwirth, S. Kappel, T. Waitz, T. Prohaska, W. Lindner, and M. Lämmerhofer, ACS Nano **7**, 1129 (2013).
[38] I. Rodriguez-Loureiro, E. Scoppola, L. Bertinetti, A. Barbetta, G. Fragneto, and E. Schneck, Soft Matter **13**, 5767 (2017).
[39] O. Löhmann, S. Micciulla, O. Soltwedel, E. Schneck, and R. von Klitzing, Macromolecules **51**, 2996 (2018).
[40] A. Andrieu-Brunsen, S. Micoureau, M. Tagliazucchi, I. Szleifer, O. Azzaroni, and G. J. A. A. Soler-Illia, Chem. Mater. **27**, 808 (2015).
[41] E. D. Bain, K. Dawes, A. E. Özcam, X. Hu, C. B. Gormand, J. Srogl, and J. Genzer, Macromolecules **45**, 3802 (2012).
[42] C. J. Galvin, E. D. Bain, A. Henke, and J. Genzer, Macromolecules **48**, 5677 (2015).
[43] Y. Li, Y. Ko, Y. Lin, D. Kiserow, and J. Genzer, Macromolecules **50**, 8580 (2017).
[44] K. A. Melzak, K. Yu, D. Bo, J. N. Kizhakkedathu, and J. L. Toca-Herrera, Langmuir **31**, 6463 (2015).
[45] E. B. Zhulina and M. Rubinstein, Macromolecules **47**, 5825 (2014).
[46] K. Matyjaszewski, M. Wei, J. Xia, and S. G. Gaynor, Macromol. Chem. Phys. **199**, 2289 (1998).
[47] H. Zhang, B. Klumperman, W. Ming, H. Fischer, and R. van der Linde, Macromolecules **34**, 6169 (2001).
[48] X. Chu, J. Yang, G. Liu, and J. Zhao, Soft Matter **10**, 5568 (2014).
[49] C. J. Galvin, M. D. Dimitrious, S. K. Satija, and J. Genzer, J. Am. Chem. Soc. **136**, 12737 (2014).
[50] A. P. Martinez, J.-M.-Y. Carrillo, A. V. Dobrynin, and D. H. Adamson, Macromolecules **49**, 547 (2016).
[51] A. Halperin and M. Kröger, Langmuir **25**, 11621 (2009).
[52] I. Adroher-Benitez, A. Moncho-Jorda, and J. Dzubiella, Langmuir **33**, 4567 (2017).
[53] J. U. Kim and B. O'Shaughnessy, Phys. Rev. Lett. **89**, 238301 (2002).